Supplemental Material: Topological flat bands from two-dimensional dipoles

Proof of uniform π/N: Here, we prove that a periodic drive pattern enables arbitrary uniform π/N flux per square plaquette, as shown in Fig. 2b of the main text. The flux in each plaquette p is the phase of the Wilson loop, $W(p) = \prod_{\partial p} t_{ij}$. For a given plaquette, p_ℓ, $\Phi_\ell = \arg[W(p_\ell)] = \arg[t_\ell^2 t_\ell'^2]$, where $t_\ell = \beta_{\ell-1} w + \beta_\ell \bar{w}$, $t'_\ell = \beta_\ell \bar{w} + \beta_{\ell+1} w$ (dropping the normalization factor which will not contribute to the argument) and $w = e^{i\pi/3}$. Taking $\theta_\ell = \arg(t_\ell)$ and $\theta'_\ell = \arg(t'_\ell)$ yields the phase of the Wilson loop as $\Phi_\ell = 2\theta_\ell + 2\theta'_\ell = 2\theta_\ell - 2\theta_{\ell+1}$. To achieve a uniform π/N flux per plaquette, we can take $\theta_{\ell+1} = \eta - \ell\frac{\pi}{2N} + a_\ell \pi$ (note that in the main text the a_ℓ term was dropped for notational simplicity), where $a_\ell \in \{0,1\}$ and $\eta \in \mathbb{R}$ is a constant to be specified. Defining $r_\ell = \beta_{\ell+1}/\beta_\ell$ yields $\beta_\ell = \prod_{k=1}^{\ell-1} r_k \beta_1$, implying that the periodicity of β is L such that $\prod_{k=1}^{L} r_k = 1$. We now prove, for all $N \in \mathbb{Z}_{>0}$, that there exists a periodic choice of β with a maximum periodicity of $4N$ which generates the desired uniform background flux. First, note that $t_{\ell+1}/\beta_\ell = r_\ell \bar{w} + w$ and hence, $\theta_{\ell+1} = \arg(r_\ell \bar{w} + w) + b_\ell \pi$, where $b_\ell \in \{0,1\}$. Simple geometry reveals that taking

$$r_\ell = \frac{\beta_{\ell+1}}{\beta_\ell} = \frac{\sin(\frac{\pi}{3} - \eta + \ell\frac{\pi}{2N})}{\sin(\frac{\pi}{3} + \eta - \ell\frac{\pi}{2N})} \tag{1}$$

ensures that $\arg(r_\ell \bar{w} + w) = \eta - \ell\frac{\pi}{2N} + c_\ell \pi$, where $c_\ell \in \{0,1\}$. Thus, we have succeeded in achieving θ_ℓ of the desired form with $a_\ell = b_\ell + c_\ell (\mathrm{mod}\ 2)$. Inspection reveals that for $N \in 3\mathbb{Z}$, $\prod_{\ell=1}^{2N} \frac{\sin(\frac{\pi}{3} - \eta + \ell\frac{\pi}{2N})}{\sin(\frac{\pi}{3} + \eta - \ell\frac{\pi}{2N})} = 1$ for all $\eta \in \mathbb{R}$, while for $N \in \mathbb{Z}\backslash 3\mathbb{Z}$, $\prod_{\ell=1}^{4N} \frac{\sin(\frac{\pi}{3} - \eta + \ell\frac{\pi}{2N})}{\sin(\frac{\pi}{3} + \eta - \ell\frac{\pi}{2N})} = 1$ for $\eta = \lambda\pi/N$ with integer λ. $\square$

As a simple example, to generate a uniform $\pi/3$ background gauge field, one can utilize a drive pattern with period $2N = 6$; with $\beta = \{1, 5, -10, \frac{5}{2}, \frac{5}{6}, \frac{2}{3}\}$ (e.g. $\eta = \tan^{-1}(\frac{1}{3\sqrt{3}}) - \pi/6$), one finds that the topological bandstructure exhibits six bands, where the lowest carries Chern number $c = -1$. We have verified that adding in further neighbor interactions (up to $1/27R_0$) does not alter the Chern number of the lowest band. While such additional interactions do indeed lead to a change in the dispersion of the band structure and hence the flatness, we find that (for the two-band models considered in the maintext) re-optimizing at each order always enables us to recover the previous flatness.

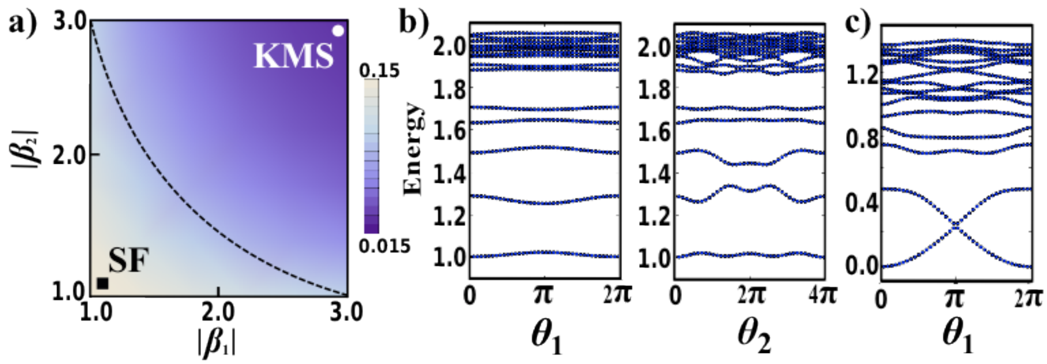

FIG. S1: **Knight's move solid.** a) Exact diagonalization at $N_s = 24$ reveals a spectral gap density plot, which varies as a function of MW drive amplitude for $(\Theta_0, \Phi_0) = (0.21, 0.42)$, $\beta_1 = 2.8e^{1.69i}$, and $\beta_2 = 2.8e^{5.63i}$. Although the MW parameters are slightly different than in the main text, the qualitative KMS phase is unchanged; this choice of parameters better illustrates the transition from a SF, which has a unique finite-size ground state, to the degenerate KMS. b) Spectral flow of the KMS ground state in the $k_1 = k_2 = 0$ momentum sector under twisting the boson boundary condition in the $\hat{g}_1$ and $\hat{g}_2$ directions for parameters indicated by the white circle in a). For the $N_s = 24$ $(3 \times 4 \times 2)$ lattice with 6 bosons, momentum sectors return to themselves after 2π in θ_1 and after 4π in θ_2. In the KMS phase, the ground state energy is insensitive to twisting. (c) This contrasts with the quadratic response of the energy in the phase-coherent SF. Depicted is the spectral flow of the $k_1 = k_2 = 0$ momentum sector under twisting in the $\hat{g}_1$ direction for parameters indicated by the black square in a).

Knight's Move Solid: The knight's move solid discussed in the maintext exhibits 4 degenerate ground states in momentum sectors $k_1 = 0, k_2 = 0, \pi/2, \pi, 3\pi/2$. As shown in Fig. S1(b), twisting the boundary condition in the $\hat{g}_1$, $\hat{g}_2$ directions (Fig. 4b) does not affect the ground state energy consistent with an insulator. By enlarging the system size, we confirm that the finite-size excitation gap of the KMS appears to remain finite in the thermodynamic limit.

As we vary the magnitude of β_1 and β_2, keeping all other parameters fixed, the spectral gap $E_1 - E_0$ changes dramatically (Fig. S1(a)), opening up as either amplitude approaches 1 (corresponding to linearly polarized MW driving). At $|\beta_1| = |\beta_2| = 1$, diagonalization reveals a unique ground state, residing in the $k_1 = k_2 = 0$ sector. While our system sizes are too small to clearly observe the Goldstone mode of a superfluid (SF), in contrast to the KMS, twisting the boundary conditions dramatically alters the ground state energy, as depicted in Fig. S1(c); this is consistent with a SF which harbors long-range phase coherence.

Optical Raman Dressing: Our proposal can also be carried out in currently available ultracold polar molecules, such as $^{40}\mathrm{K}^{87}\mathrm{Rb}$, $^{7}\mathrm{Li}^{133}\mathrm{Cs}$, and $^{41}\mathrm{K}^{87}\mathrm{Rb}$. Spatial modulation of the bright state can be achieved by utilizing optical Raman beams to dress the rotational states of each molecule. For the upper leg of the Raman transition, we propose to utilize the $|J', m'\rangle = |2, 2\rangle$ rotational states of the $v' = 41$ vibrational level of the $(3)^1\Sigma^+$ electronic state. These states harbor a strong 640 nm transition to the ground state and enable modulation of the bright state at lattice length scales.